Human carbonyl reductase 1 as efficient catalyst for the reduction of glutathionylated aldehydes derived from lipid peroxidation.

Rossella Rotondo[a#], Roberta Moschini[a#], Giovanni Renzone[#b], Tiziano Tuccinardi[c], Francesco Balestri[a], Mario Cappiello[a], Andrea Scaloni[b], Umberto Mura[a] and Antonella Del-Corso[a]

[a]University of Pisa, Department of Biology, Biochemistry Unit, via S. Zeno, 51, Pisa (Italy);

[b]Proteomics & Mass Spectrometry Laboratory, ISPAAM-CNR, via Argine, 1085, Napoli, (Italy);

[c]University of Pisa, Department of Pharmacy, via Bonanno, 6, Pisa (Italy).

# These authors contributed equally to the work.

*****Corresponding author: Antonella Del-Corso, University of Pisa, Department of Biology, Biochemistry Unit, via S. Zeno, 51, 56123, Pisa, Italy.

Phone: +39.050.2211454; Fax: +39.050.2211460

E-mail: antonella.delcorso@unipi.it

Abstract

Human recombinant carbonyl reductase 1 (E.C. 1.1.1.184, hCBR1) is shown to efficiently act as aldehyde reductase on glutathionylated alkanals, namely 3-glutathionyl-4-hydroxynonanal (GSHNE), 3-glutathionyl-nonanal, 3-glutathionyl-hexanal and 3-glutathionyl-propanal. The presence of the glutathionyl moiety appears as a necessary requirement for the susceptibility of these compounds to the NADPH-dependent reduction by hCBR1. In fact the corresponding alkanals and alkenals, and the cysteinyl and γ-glutamyl-cysteinyl alkanals adducts were either ineffective or very poorly active as CBR1 substrates. Mass spectrometry analysis reveals the ability of hCBR1 to reduce GSHNE to the corresponding GS-dihydroxynonane (GSDHN) and at the same time to catalyze the oxidation of the hemiacetal form of GSHNE, generating the 3-glutathionylnonanoic–δ-lactone. These data are indicative of the ability of the enzyme to catalyze a disproportion reaction of the substrate through the redox recycle of the pyridine cofactor. A rationale for the observed preferential activity of hCBR1 on different GSHNE diastereoisomers is given by molecular modelling. These results evidence the potential of hCBR1 acting on GSHNE to accomplish a dual

role, both in terms of HNE detoxification and, through the production of GSDHN, in terms of involvement into the signalling cascade of the cellular inflammatory response.

Key words: carbonyl reductase 1; 3-glutathionyl-4-hydroxynonanal; hydroxynonenal detoxification; 4-hydroxy-2-nonenal;

Abbreviations: 3-glutathionyl-1,4-dihydroxynonane: GSDHN; 3-glutathionyl-4-hydroxynonal: GSHNE; 3-glutathionyl-4-hydroxynonanoic-δ-lactone: GSHNA-lactone; 4-hydroxy-2-hexenal: HHE; 4-hydroxy-2-nonenal: HNE; 4-oxo-*trans*-2-nonenal: ONE; 9,10-PQ: 9,10-phenanthrenquinone; BSA: bovine serum albumin; carbonyl reductase 1: CBR1; extracted ion chromatograms: EIC; dimethyl sulfoxide: DMSO; D,L-dithiotreitol: DTT; human recombinant carbonyl reductase 1: hCBR1; interval of retention time: ΔRT; isopropyl-β-D-thiogalactopyranoside: IPTG; Met-Arg-Phe-Ala peptide: MRFA; molecular dynamic: MD; prostaglandin: PG; sodium dodecyl sulphate: SDS; total ion chromatogram: TIC;

Introduction

Lipid peroxidation is considered as a toxic consequence of oxidative stress, due to the generation of highly reactive saturated and unsaturated aldehydes, such as acrolein, malondialdehyde, 4-hydroxy-2-nonenal (HNE), 4-hydroxy-*trans*-2-hexenal (HHE) and *trans*-2-nonenal [1,2]. These compounds are involved in the development of several pathological conditions [1-3], associated with the formation of corresponding adducts with proteins and nucleic acids. Studying their cellular detoxification mechanism is thus important. The main enzymes involved in the detoxification pathway are glutathione S-transferases (GSTs) [4], which are responsible for the conjugation of unsaturated aldehydes with glutathione (GSH), aldehyde dehydrogenases [5-8], aldo-keto reductases [5,9-11], alcohol dehydrogenases [5,12] and cytochromes P450 [5,13-15]. In particular, members of aldo-keto reductases family, such as AKR1B1 [9,10] and AKR1B10 [11], and of the short chain dehydrogenase/reductases family, such as carbonyl reductase 1 (CBR1) [16,17] have been reported to efficiently transform the above mentioned aldehydes and/or their glutathionylated adducts.

Carbonyl reductase 1 [E.C. 1.1.1.184] is a monomeric NADPH-dependent enzyme of 277 amino acids widely diffused in mammals [18]. In humans, it has been found in the brain, liver, kidney, stomach, small intestine, and epidermis [19,20]. In terms of its reductase activity, the enzyme has a broad substrate specificity on various carbonyl substrates, showing a marked activity towards *orto*

or *para* xenobiotic quinone derivatives (e.g., 9,10-phenanthrenequinone or menadione) but also towards endogenous substrates, such as eicosanoids, steroids and lipid derived carbonyl compounds [21-23].

Even though the potential of CBR1 to reduce aldehydes has been reported, aldehydes, among carbonyl compounds, are poor substrates for human CBR1 [23]. The case of 4-oxo-*trans*-2-nonenal (ONE) is indicative, as it carries both an oxo and an aldehyde group; ONE has been reported to be efficiently reduced at the oxo group thus generating HNE, with only a marginal reduction (approximately 10%) of the aldehydic moiety [17]. In fact, Doorn et al. associated the possibility for the aldehydic group to be reduced by CBR1 with the simultaneous presence in the molecule of both the aldehydic carbonyl and the oxo groups.

The recognition of carbonyl compounds as a substrate by CBR1 seems to be dependent on the presence of Cys^{227}, which is a reactive cysteine located in the proximity of the substrate-binding site, and suggested as being involved in the correct substrate orientation [24]. The residues Trp^{229}, Ala^{235} and Met^{241} also appear to be important in the appropriate allocation of the hydrophobic moieties of substrates into the active site [23]. Near the active site, a glutathione-binding site has also been identified [25, 26], which is involved in the recognition of glutathionylated substrates.

The relevance of the glutathione moiety in the recognition of potential substrates by CBR1 was reported for the first time in a study on prostaglandin (PG) metabolism. The reduction of the 9 keto group of PGA_1 occurred only for the glutathione adduct of PGA_1 ($GSPGA_1$), and was almost negligible for the free PGA_1 [25, 27]. Conversely, both menadione and glutathionylated-menadione (GS-menadione) were comparable as reductable CBR1 substrates [27]. In addition, $GSPGA_1$ and GS-menadione were shown to be efficient inhibitors of the 15-hydroxyprostaglandin dehydrogenase activity of CBR1 on PGB_1 [27].

The Cys^{227} residue does not appear to be very critical in the binding of glutathionylated molecules. Thus, the C227S CBR1 mutant, while inactive in terms of menadione reduction, is still active, in fact more active than the wild type enzyme, on GS-menadione [24]. Similar results have been obtained when PGA_1 and $GSPGA_1$ were compared as substrates for the C227S CBR1 mutant [24]. These findings highlight the strong addressing effect exerted by the glutathionyl moiety of the substrates for their correct allocation within the active site. One exception was observed for S-nitrosoglutathione, which is efficiently reduced by CBR1 [26], and for which a prominent role of Cys^{227}, but not of the glutathione-binding site, in its susceptibility to reduction has been established [28].

A new glutathionylated substrate of CBR1, 3-glutathionyl-4-hydroxynonal (GSHNE), has recently been reported [29]. The enzyme was demonstrated to act as an efficient $NADP^+$ -dependent

dehydrogenase able to oxidize GSHNE to the corresponding 3-glutathionyl-4-hydroxynonanoic-δ-lactone (GSHNA-lactone). The present work shows the ability of CBR1 to catalyze an efficient NADPH-dependent reduction of glutathionylated aldehydes. In the presence of CBR1, GSHNE can therefore undergo a divergent redox transformation, ending with the generation of the oxidation as well as the reduction product through a disproportion reaction. This evidence reinforces the prominent role of CBR1 in the metabolism of lipid peroxidation products.

Materials and Methods

Materials

9,10-phenanthrenquinone (9,10-PQ), bovine serum albumin (BSA), cysteine, CysGly, dimethyl sulfoxide (DMSO), D,L-dithiotreitol (DTT), γGluCys, 5,5'-dithiobis-(2-nitrobenzoicacid), GSH, hexanal, isopropyl-β-D-thiogalactopyranoside (IPTG), Met-Arg-Phe-Ala peptide (MRFA), $NADP^+$, N-acetyl-cysteine, nonanal, propanal, protease inhibitors cocktail, sodium dodecyl sulphate (SDS), *trans*-2-hexenal, *trans*-2-nonenal, *trans*-2-propenal (acrolein) were purchased from Sigma–Aldrich (St. Louis, MO, USA). HHE was purchased from Cayman Chemicals (AnnArbor, MI, USA). Whatman DEAE-cellulose (DE-52) and Sephacryl S200 were purchased from GE Healthcare (Little Chalfont, UK). Blue Sepharose and Bradford reagent were purchased from Bio-Rad (Hercules, CA, USA). YM10 membranes (10 kDa cut-off) were purchased from Amicon Millipore (Darmstadt, Germany). Dialysis tubing (10 kDa cut-off) was purchased from Spectrum Laboratories (Rancho Dominguez, CA, USA). All inorganic chemicals were of reagent grade from BDH (VWR International, Poole, Dorset, UK). All solvents were HPLC grade from J.T. Baker Chemicals (Center Valley, PA, USA). NADPH was from Carbosynth (Compton, England).

RNA extraction and cDNA synthesis. Total RNA was extracted from a human astrocytoma cell line (ADF) with TRI® Reagent (Sigma), following the manufacturer's instructions. cDNA was prepared from total RNA by reverse transcription, using 200 units of Super Script™ III Reverse Transcriptase (Invitrogen) and 0.5 µg of an oligo-dT primer in a final volume of 50 µl. The mixture also contained 0.5 mM of each dNTP (GE-Healthcare), 75 mM KCl, 3 mM $MgCl_2$, 10 mM DTT and 0.1 mg/ml BSA in 50 mM Tris-HCl, pH 8.3. This reaction mixture was incubated at 42 °C for 60 min. The product was directly used for PCR amplification or stored at -20 °C. As reported [29], the corresponding cDNA sequence completely matched with the human wild type counterpart.

Polymerase chain reaction. Aliquots of 1 µl of crude cDNA were amplified in a Bio-Rad Gene Cycler™ thermocycler, using 2.5 units of *Thermus aquaticus* DNA polymerase (GE-Healthcare), 1 mM of each dNTP (GE-Healthcare), 1 µM of each PCR primer, 50 mM KCl, 2.5 mM $MgCl_2$ and 0.1 mg/ml BSA in 10 mM Tris-HCl, pH 8.3, containing 0.1% v/v Triton X-100. At the 5'-end, we used the specific primer 5'-CAT ATG TCG TCC GGC ATC CAT GT-3', which corresponds to the sequence encoding the first six amino acids of the mature protein and containing an Nde I restriction site for ligation into the expression vector, and at the same time provided the ATG codon for an additional methionine at position 1. At the 3'-end, the specific primer: 5'-GAA TTC CTA CCA CTG TTC AAC TCT CTT-3' encoded the last six amino acids, followed by a stop codon and an Eco RI restriction site. After an initial denaturation step at 95 °C for 5 min, we performed 35 amplification cycles (1 min at 95 °C, 30 sec. at 50 °C, 1 min at 72 °C), which were followed by a final step of 7 min at 72 °C. An amplification product of about 800 bp was obtained, in agreement with the expected size (831 bp).

Cloning and sequencing. The crude PCR product was ligated into a pGEM (Promega) vector without further purification, using a 1:5 plasmid to insert molar ratio and incubating the mixture overnight, at room temperature. After transformation of *E.coli* XL-1 Blue competent cells with the ligation product, positive colonies were selected by PCR using the plasmid primers SP6 and T7, and were grown in LB/ampicillin medium. DNA was extracted using the Plasmid MiniPrep Kit (Euroclone) and custom sequenced at Eurofins MWG, Ebersberg, Germany.

Cloning in expression vector. pGEM plasmid containing the appropriate sequence was digested with Nde I and Eco RI restriction enzymes for 2 h at 37 °C and the digestion product was separated on agarose gel. The fragment obtained was purified from gel using the QIAEX II Extraction kit (Qiagen) and ligated into the expression vector pET30 (Novagen, Darmstadt, Germany), which was previously linearized with the same enzymes. The resulting plasmid was sequenced and shown to encode the mature protein.

Expression and purification of the recombinant protein. For the expression of human recombinant protein (hCBR1), the pET30 vector, containing the nucleotide sequence encoding human carbonyl reductase 1, was used to transform BL21(DE3)pLysS *E. coli* cells. Protein expression was induced by the addition of 0.4 mM IPTG at a cell culture that reached an $O.D._{600}$ value of 0.8. Cells were grown at 37 °C overnight and then harvested at 2,000 x *g* for 30 min at 4 °C. Cells were then resuspended in 10 mM sodium phosphate buffer, pH 7.0, supplemented with 2 mM DTT and

protease inhibitors cocktail, and sonicated. After centrifugation at 15,300 x *g* for 30 min at 4 °C, the expressed protein was obtained in a soluble form. The enzyme was purified to electrophoretic homogeneity (Fig. 1S, supplementary material) using a combination of anionic exchange and affinity chromatography as previously described for the human astrocytoma cell enzyme [29]. The purified enzyme (50 U/mg) was stored in 10 mM sodium phosphate buffer pH 7.0 containing 0.1 mM $NADP^+$, 1.5 M NaCl, 2 mM DTT and 31% (v/v) glycerol at -80°C; it was extensively dialyzed against 10 mM sodium phosphate buffer, pH 7.0, before use.

Enzyme assays of hCBR1. The activity of hCBR1 was determined at 37 °C using GSHNE as a substrate to be oxidized. The reaction was monitored following the increase in absorbance at 340 nm due to the reduction of $NADP^+$ (ε_{340}= 6.22 mM^{-1} cm^{-1}). The reaction mixture contained 0.1 mM GSHNE, 0.18 mM $NADP^+$ in a 50 mM sodium phosphate buffer, pH 8.4.

One unit of enzyme activity is the amount that catalyzes the conversion of 1 μmol of substrate/min in the above assay conditions.

The NADPH-dependent reductase activity of hCBR1 was determined at 37 °C by monitoring the decrease in absorbance at 340 nm due to the oxidation of 0.18 mM NADPH in 50 mM sodium phosphate, pH 6.0 in the presence of the indicated substrates. The 9,10-phenanthrenequinone stock solutions were prepared in DMSO and when this compound was used as substrate for CBR1 the assay mixture contained DMSO at the fixed final concentration of 2 % (v/v). This DMSO concentration had no effect on the activity of hCBR1, as measured under standard conditions.

Synthesis of aldehydes. Diethyl acetal of HNE was prepared as previously described [29]. Free aldehyde was prepared by acid hydrolysis (pH 3.0) of the diethylacetal for 1 h, at 4 °C. The concentration of HNE and *trans*-2-nonenal was determined by measuring the absorbance at 224 nm and 228, respectively, using an extinction coefficient of 13.7 mM^{-1} cm^{-1} [30]. HHE and *trans*-2-hexenal concentrations were determined spectrophotometrically at 224 and 220 nm using extinction coefficients of 13.7 [31] and 18.1 ± 0.3 mM^{-1} cm^{-1} (obtained using known concentrations of the aldehydes), respectively.

Preparation of thiol-adducts. The adducts were prepared by incubating reduced thiol compounds with different aldehydes at 1.5:1 molar ratio in 50 mM sodium phosphate buffer pH 7.4 at 37 °C for 1 h, followed by an overnight incubation at 4°C. The reaction was monitored by measuring the consumption of the free aldehyde, as described above, and the residual reduced thiol by the Ellman assay [32]. In all cases, taking into account the spontaneous oxidation of the SH moiety, a

stoichiometric consumption of the thiol and free aldehyde was observed. In addition, the residual free aldehyde accounted for no more than 10% of the initial value, a concentration that did not exert any effect on the enzymatic activity of hCBR1 (data not shown). The amount of residual acrolein and trans-2-hexenal required a further purification step of the adducts on Bond-Elut C18 (Agilent Technologies). The concentration of these adducts was evaluated by enzymatic titration. The adducts were stored at -80 °C, until used.

3-Glutathionyl-1,4-dihydroxynonane (GSDHN) was prepared incubating GSHNE with a 20-fold molar excess of $NaBH_4$. After 24 h, the reaction was quenched by slowly adding 1 M HCl on ice to achieve a final pH value of 7.0. The 1,4-dihydroxynonane generated through the reduction of the residual HNE present in the GSHNE preparation (see above) did not exert any effect on the enzymatic activity of hCBR1.

Mass spectrometry analysis of the reaction products deriving from the hCBR1 catalyzed transformation of GSHNE. A sample containing 50 μM GSHNE, 20 μM NADPH, 33 μM GSH, 5.5 μM HNE in 50 mM phosphate buffer, pH 6.2, was incubated with 94 mU/ml hCBR1 at 37 °C. The extent of reaction was examined by sampling, on a time-course basis, the reaction mixture at different reaction times. In particular, samples 1 to 12 were withdrawn at 0, 1, 2, 3, 5, 10, 15, 25, 40, 60, 90, and 120 min of incubation, respectively. In parallel, identical samples containing isolated components in 50 mM phosphate buffer, pH 6.2, *i.e.* 50 μM GSHNE, 20 μM NADPH, 33 μM GSH, 5.5 μM HNE, or 94 mU/ml hCBR1, or mixtures of these compounds, were incubated at 37 °C. After sampling, the reaction mixtures were immediately frozen in dry ice, then lyophilized and stored at -80 °C, until subsequent use. The samples were then solubilized in 0.1% trifluoroacetic acid and analysed by nLC-ESI-LIT-MS/MS, using an LTQ XL mass spectrometer equipped with a Proxeon nanospray source, which was connected to an UltiMate 3000 RSLC nano-liquid chromatographer (ThermoFisher, U.S.A.). Firstly, samples were separated on a 75 μm I.D. x 15 cm column, packed with Acclaim PepMap RSLC C18, 2 μm, 100 Å (ThermoFisher, U.S.A.). Mobile phases were 0.1% (v/v) aqueous formic acid (solvent A) and 80% acetonitrile, 0.1% (v/v) aqueous formic acid (solvent B), running at total flow rate of 300 nl/min. A linear gradient was initiated after sample loading; solvent B ramped from 3 % to 10 % over 7 min, from 10 to 40 % over 30 min, and from 40 to 80 % over 5 min. Spectra were acquired in the range *m/z* 300−800. Sample were analysed under collision-induced dissociation (CID)-MS/MS data-dependent product ion scanning procedure, enabling dynamic exclusion (repeat count 1 and exclusion duration 60 s) over the three most abundant ions. Mass isolation window and collision energy were set to *m/z* 3 and 35%, respectively.

Raw data from nLC-ESI-LIT-MS/MS analyses were manually interpreted and assigned to specific glutathione derivatives (data not shown). A semi-quantitative measurement of the reaction products was achieved by analysing the same samples by nLC-ESI-LIT-MS, as already described for the MS/MS experiments, with the unique exception that chromatographic runs were acquired in MS scan mode without ion fragmentation [33, 34]. In this case, extraction and integration of the LC-MS peaks corresponding to the reagent GSHNE and to the observed reaction products were manually performed in the same total ion chromatogram, using to this purpose the Genesis algorithm within the Xcalibur software (version 2.0.7 SP1, ThermoFisher, U.S.A.). Since the species under investigation were expected to have different ionization properties, a measurement of their relative amounts was gained by extracting and byintegrating peaks corresponding to these compounds and to peptide MRFA (*exp*. and *theor*. MH^+ values at *m/z* 524.31 and 524.26, respectively), which was used as internal reference and spiked in all samples at the same concentration before each MS analysis. Semi-quantitative evaluation of the modification extent was then determined by calculating the following ratio: peak area $_{\text{species of interest}}$/peak $_{\text{area internal reference peptide}}$. This procedure was applied to all samples reported above by carrying out experiments in quintuplicate.

Docking calculations. The crystal structure of hCBR1 (pdb code 3BHJ [26]) was taken from the Protein Data Bank [35]. After adding hydrogen atoms, the protein was minimized using Amber14 software [36] and ff14SB force field at 300 K. The complex was placed in a rectangular parallelepiped water box, an explicit solvent model for water, TIP3P, was used and the complex was solvated with a 10 Å water cap. Sodium ions were added as counter ions to neutralize the system. Two steps of minimization were then carried out; in the first stage, we kept the protein fixed with a position restraint of 500 kcal/mol $Å^2$ and we solely minimized the positions of the water molecules. In the second stage, we minimized the entire system through 5000 steps of steepest descent followed by conjugate gradient (CG) until a convergence of 0.05 kcal/Å mol. The ligands were built using Maestro [37] and were minimized by means of Macromodel [38] in a water environment using the CG method until a convergence value of 0.05 kcal/Å mol, using the MMFFs force field and a distance-dependent dielectric constant of 1.0. The region of interest used by the docking program GOLD version 5.1 [39] was defined in order to contain the residues within 10 Å from the original position of the ligand in the X-ray structure. The 'allow early termination' option was deactivated, while the possibility for the ligand to flip ring corners was activated. The remaining GOLD default parameters were used, and the ligands were submitted to 30 genetic algorithm runs. The docking analysis was carried out using the ChemScore fitness function. Cluster analysis was performed on the results using an RMSD tolerance of 2.0 Å and the best-ranked pose

leading to the interaction of the cyclic hemiacetal with the catalytic triad of the active site (S140, Y194 and K198) was taken into account.

Molecular Dynamic (MD) simulations. All simulations were performed using AMBER, version 14 [36]. MD simulations were carried out using the ff14SB force field at 300 K. The complex was placed in a rectangular parallelepiped water box. An explicit solvent model for water, TIP3P, was used, and the complexes were solvated with a 20 Å water cap. Chlorine ions were added as counterions to neutralize the system. Prior to MD simulations, two steps of minimization were carried out using the same procedure described above. Particle mesh Ewald electrostatics and periodic boundary conditions were used in the simulation [40]. The MD trajectory was run using the minimized structure as the starting conformation. The time step of the simulations was 2.0 fs with a cutoff of 10 Å for the non-bonded interaction, and SHAKE was employed to keep all bonds involving hydrogen atoms rigid. Constant-volume periodic boundary MD was carried out for 0.5 ns, during which the temperature was raised from 0 to 300 K. Then 30 ns of constant pressure periodic boundary MD was carried out at 300 K using the Langevin thermostat to maintain constant the temperature of our system. All the α-carbons of the protein were blocked with a harmonic force constant of 10 kcal/mol $Å^2$. General Amber force field parameters were assigned to the ligands and cofactor, while partial charges were calculated using the AM1-BCC method as implemented in the Antechamber suite of AMBER 14. The final structures of the complexes were obtained as the average of the last 30 ns of MD minimized by the CG method, until a convergence of 0.05 kcal/mol $Å^2$. The average structures were obtained using the Cpptraj program [41] implemented in AMBER 14.

Other methods. Protein concentration was determined according to Bradford [42]. SDS-PAGE was performed according to Laemmli [43]; gels were stained according to the silver staining technique [44]. K_M and k_{cat} values were determined by non-linear regression analysis of the kinetic data using GraphPad software. The k_{cat} values were calculated on the basis of a hCBR1 mass value of 30,375 Da.

Results

Kinetic characterization of hCBR1 as a dehydrogenase. Native hCBR1 was expressed in BL21(DE3)pLysS *E. coli* cells and purified to electrophoretic homogeneity (Fig. 1S, supplementary material) thereby obtaining an enzyme preparation with a specific activity of 50 U/mg of protein.

The $NADP^+$-dependent GSHNE oxidation catalyzed by hCBR1 was kinetically characterized. The non-linear regression analysis of the kinetic data in Fig. 1 led to an estimation of K_M for GSHNE and $NADP^+$ of 27.2 ± 1.0 μM and 5.9 ± 0.4 μM, respectively, which were comparable to those previously reported for the enzyme purified from ADF cells [29]. From the same analysis, we measured k_{cat} values of 2,000 ± 56 min^{-1} and of 1,566 ± 56 $min^{-1}$from data of GSHNE and $NADP^+$ as variable substrates, respectively. These values are approximately 5-fold higher than that previously measured for the enzyme purified from ADF [29]. Even though less efficiently than GSHNE, also GSHHE is recognized as substrate to be oxidized by hCBR1, with a K_M and a k_{cat} of 76.7 ± 5.9 μM and 924 ± 37 min^{-1}, respectively.

Gamma-glutamylcysteinyl-HNE and cysteinyl-HNE were used as substrates in order to assess the relevance of the integrity of the glutathionyl moiety of GSHNE to the oxidation of the aldehyde. With these compounds as substrates either no activity or merely approximately 5 % of the activity measured with GSHNE was observed, respectively.

The hCBR1 was inactive towards a number of different alkanals and alkenals that were tested as potential substrates; they include propanal, hexanal, nonanal, *trans*-2-propenal, *trans*-2-hexenal, *trans*-2-nonenal, HHE and HNE.

hCBR1 as a reductase for glutathionylated-aldehydes. As expected, the hCBR1 reduced 9,10-PQ, with a specific activity of 117 U/mg. A number of aldehydes, such as propanal, hexanal, nonanal, *trans*-2-propenal, *trans*-2-hexenal, *trans*-2-nonenal and HHE were tested as substrates of hCBR1; they were not reduced in the adopted assay conditions. On the other hand, the glutathionylated-adducts derived from the above alkenals, namely GS-propanal, GS-hexanal and GS-nonanal, were very efficiently reduced by hCBR1. The kinetic parameters for the NADPH-dependent reductase activity of hCBR1 for the different GS-aldehydes were determined. From the data shown in Tab. 1, GS-nonanal appeared to have the strongest affinity for hCBR1, with a K_M value of 6.5 ± 0.4 μM and a k_{cat} of 1,848 ± 83 min^{-1}. GS-hexanal and GS-propanal, although less effective than GS-nonanal, were still good substrates (Table 1), with a K_M and k_{cat} of 23.8 ± 2.7 μM and 1,830 ± 101 min^{-1} and of 20.7 ± 1.8 μM and 1,140 ± 46 min^{-1}, respectively. As observed for the dehydrogenase activity of hCBR1, the integrity of the glutathionyl moiety of the adducts appears relevant for substrate recognition. In fact with Cys-nonanal and γ-glutamylcysteinyl-nonanal as substrates either no activity was observed or merely approximately 14 % of the activity measured with GS-nonanal, respectively.

As expected for a pyridine cofactor-linked reaction, the reductase activity of hCBR1 was strongly affected by the pH value of the medium. An approximate 5-fold decrease in the NADPH-dependent

reduction of GS-nonanal was observed when moving from pH 6 to 8.4. On the other hand, a parallel increase was observed for the $NADP^+$-dependent oxidation of GSHNE in the same range of pH values (Fig. 2).

GSHNE as substrate for the dehydrogenase/reductase activity of hCBR1. The susceptibility of GSHNE to the $NADP^+$-dependent oxidation catalyzed by hCBR1 has been previously assessed [29]. In this study, the proneness of GSHNE to be reduced by hCBR1 was monitored by nLC-ESI-LIT-MS analysis under acidic pH conditions (pH 6.2), minimizing the dehydrogenase activity of the enzyme (Fig. 2). nLC-ESI-LIT-MS/MS analysis of both standard compounds and the reaction mixtures previously mentioned (samples 1 to 12, see Methods) was able to identify initial reagents and glutathione derivatives that gradually appeared after hCBR1 addition (data not shown). As an example, Fig. 3 displays the total ion chromatogram (TIC) for the reaction mixture withdrawn at 5 min of incubation (Panel A), and the extracted ion chromatograms (EIC) corresponding to the different HNE-bearing glutathione derivatives identified by MS/MS (Panels B to F). A series of peaks showing the same mass values were detected (peaks 1, 2 and 3), which were referred to GSHNE (*exp*. and *theor*. MH^+ values at *m/z* 464.25 and 464.21, respectively, within the interval of retention time (ΔRT) = 30.9-34.1 min) (Fig. 3B). These peaks were related with pairs of unresolved diastereomers, among the eight different compounds (Fig. 1S, supplementary material) generated considering the presence of different chiral centres in these HNE-bearing glutathione derivatives, as already reported in the case of GSHNE [29, 45, 46] and other HNE–thiol adducts [47, 48]. In particular, two of the four anomeric couples could be separated, $\mathbf{I_{S/R}}$ and $\mathbf{IV_{S/R}}$ (peaks 1 and 3, respectively). On the other hand, the couples $\mathbf{II_{S/R}}$ and $\mathbf{III_{S/R}}$ remained unresolved and eluted as peak 2. In general, GSHNE showed a progressive disappearance during the incubation with the enzyme (Fig. 4 Panel A). Out of the three peaks referred to the anomeric couples of GSHNE, peaks 2 and 3 showed a faster rate of consumption than peak 1 during the time-course monitoring (Fig. 5). On the other hand, a parallel increase of both the oxidation and reduction products, namely GSHNA-δ-lactone (*exp*. and *theor*. MH^+ values at *m/z* 462.23 and 462.19, respectively, in the interval of ΔRT = 38.0-40.1 min) and GSDHN (*exp*. and *theor*. MH^+ values at *m/z* 466.25 and 466.22, respectively, within ΔRT = 31.3-33.2 min), was observed over time (Fig. 4C and 4B, respectively. As also shown in Fig 4D, a very modest generation of the lactone hydrolysis product (*exp*. and *theor*. MH^+ values at *m/z* 480.24 and 480.20, respectively, within ΔRT = 32.8-34.4 min) and of its oxidation product at the hydroxyl group in position 4 (*exp*. and *theor*. MH^+ values at *m/z* 478.23 and 478.19, respectively, within ΔRT = 34.7-34.8 min) were also detected. Thus, despite the initially imposed reducing conditions (*i.e.* NADPH) and the acidic pH value of the medium, the

dehydrogenase activity of hCBR1 on GSHNE could take place. It is worth noting that an extensive, if not complete, transformation of GSHNE occurred at the sub-stoichiometric level of the cofactor, whose redox recycle supported a disproportion reaction of the substrate.

Specificity of hCBR1 towards GS-HNE diastereoisomers. In order to account for the apparent marked reduced transformation rate of the **I$_{S/R}$** anomeric couple (*i.e.* peak 1, Fig. 5), the eight GSHNE diastereoisomers were docked into the hCBR1 binding site using GOLD docking software with the ChemScore fitness function [49]. For each compound, the best-ranked pose leading to the interaction of the cyclic hemiacetal with the catalytic triad of the active site (S140, Y194 and K198) was taken into account.

Most of the compounds showed the hydroxyl group of the cyclic hemiacetal that formed two H-bonds with S140 and Y194 (Fig. 3S, supplementary material). The only two exceptions were compounds **I$_S$** and **II$_S$** (Fig. 6), which showed a different disposition of the cyclic hemiacetal having the lack of the H-bond with S140. These eight hCBR1-ligand complexes were subjected to 30.5 ns of MD simulation. The analysis of the MD simulation for the different hCBR1-ligand complexes highlighted that, with the exception of compound **I$_S$**, all the compounds showed stable H-bond interactions with the catalytic residues of the enzyme. In fact, in order to maintain the lipophilic interaction of the pentane substituent with W230, the cyclic hemiacetal of anomer **I$_S$** was shifted by about 3.0 Å, thus losing the interaction with Y194 and forming a stable H-bond only with S140 (Fig. 6). After about 3 ns, the cyclic hemiacetal of **I$_S$** shifted towards the solvent accessible part of the binding site, losing all the interactions with the catalytic residues and maintaining only the lipophilic interactions of the pentane group with W230 (Fig. 6, see also Table 1S, supplementary material).

Effect of GSDHN on GSHNE dehydrogenase activity of hCBR1. GSDHN, the product of the reduction of GSHNE by hCBR1, exerted an effective competitive inhibition on GSHNE oxidation (Fig. 7), with a K_i value of 12.6 ± 1.2 μM. When GS-nonanal, which is an appreciably good analogue of the open chain form of GSHNE, was used as substrate to be reduced, GSDHN exerted a rather lower inhibitory effect (IC_{50} approximately 70 μM, data not shown).

Discussion

Recent evidence that CBR1 purified from a human astrocytoma cells line was able to efficiently act as a dehydrogenase on GSHNE, thus generating the GSHNA-δ-lactone [29], highlights the

significant role of this enzyme in the detoxification pathways of cytotoxic lipid peroxidation derivatives. Making use of a highly purified human recombinant CBR1 preparation, the redox ability of the enzyme was further investigated in order to assess whether the oxidation of GSHNE was the only possible transformation process catalysed by the enzyme on this substrate. In agreement with the previously reported low reductase activity of CBR1 on aldehydic compounds (see Introduction section), hCBR1 was unable to reduce a number of alkanals and alkenals. However as with GS-propanal, GS-hexanal and GS-nonanal, inserting a glutathionyl moiety into these molecules made them very good reducible substrates for the enzyme. Such an evidence extends on the reported observation on CBR1 for its preferential action on glutathionylated-adducts of oxo carbonyl compounds [24, 25]. It reveals, for what we believe is the first time, the ability of the human enzyme to specifically act as glutathionylated-aldehyde reductase. A correlation appears between the enzyme efficiency and the hydrophobic chain length of the substrate. In fact, GS-nonanal, the compound whose structure is the most similar, among the tested adducts, to the open free aldehyde form of GSHNE, was found to have the strongest affinity for hCBR1, and also the highest specificity constant (Table 1). An approximately fourfold and fivefold decrease in the k_{cat}/K_M value with respect to GS-nonanal was observed for GS-hexanal and GS-propanal, respectively. The enzyme affinity for GS-aldehyde adducts was comparable to that reported for the best-known endogenous glutathionylated substrate of hCBR1, *i.e.* S-nitroso-glutathione (K_M approximately 30 μM) [26, 28]. The measured kinetic parameters for NADPH, using GS-nonanal as a substrate (Table 1), were also in line with the literature data obtained using menadione as a substrate to be reduced [50].

As mentioned above, the presence of a glutathione binding site in CBR1 is relevant in addressing the allocation of oxo carbonyl substrates within the active site [25]. This may obviously represent the rational for the strong effect exerted by the glutathionyl moiety of aldehydes on their reduction. In this regard the integrity of the glutathionyl moiety of the glutathionylated-aldehydes appears relevant for their eligibility as substrates of hCBR1. In fact a very low activity, if any, was measured when γ-glutamylcysteinyl-nonanal and cysteinyl-nonanal were used as substrates.

The NADPH–dependent activity of hCBR1 on GS-nonanal opens up a novel scenario in the detoxification of glutathionylated aldehydes generated during oxidative stress. Due to the structural analogy between the GS-nonanal and GSHNE open chain, hCBR1, and not only AKR1B1 is very likely to be involved in the reduction pathway of GSHNE generating GSDHN, which is a well assessed element of molecular signalling that activates the NF-kB response cascade [51,52]. As occurs for AKR1B1, the possibility of hCBR1 to reduce the carbonyl group of GSHNE, should be limited by the rather low relative amount (approximately 5%) of the free aldehyde in equilibrium

with the corresponding hemiacetal. On the other hand, the dehydrogenase activity of hCBR1, acting on the hemiacetal hydroxyl group of GSHNE, should essentially operate at the nominal concentration of the substrate.

The ability of hCBR1 to intervene bidirectionally on GSHNE was demonstrated through a mass spectrometry approach, by monitoring the redox process in a pH 6.2 condition, thus enabling both the reductive and oxidative transformation of GSHNE to occur. Indeed, both GSHNA-δ-lactone and GS-DHN accumulate, while a parallel disappearance of GSHNE occurs (Fig. 4).

In the adopted conditions, NADPH was used at a substoichiometric level. This implies that CBR1 catalyzes a disproportion reaction between the hemiacetal and the open aldehyde form of GSHNE through the redox recycle of the pyridine cofactor. Thus, a spectrophotometric monitoring at 340 nm would not be an efficient means to evaluate the reductase activity on GSHNE. This is also true for other glutathionyl adducts of 4-hydroxylalkenals, such as GSHHE.

The ability of hCBR1 to act on GSHNE does not appear to apply to all the stereoisoforms present in the GSHNE preparation. In fact, the molecular docking of different GSHNE diastereoisomers on hCBR1 and the molecular dynamic analysis of the substrate-enzyme complexes indicated that the failure in activity appears to be confined to compound $\mathbf{I_S}$ (Fig. 1S), which is the only one unable to stably interact with the catalytic residues of the enzyme.

This evidence provided a rational basis for the lower susceptibility to the transformation of Peak 1 (Fig. 5). In fact, as the $\mathbf{I_R}$ anomer is very compatible with a stable interaction with hCBR1, the enzyme action must deal with the anomeric equilibrium in order to succeed. It could be argued that these considerations are limited to the oxidative branch of the GSHNE redox transformation, since the open chain of all diastereoisomers devoid of steric restrictions in their binding.

A very effective inhibition by different glutationylated adducts has been reported for both the reduction of 9,10-phenantrenquinone and the oxidation of PGB_1 [27]. Worth mentioning is the fact that in our experiments GSDHN, the reaction product of the reductive reaction branch of GSHNE, resulted an efficient competitive inhibitor of the hCBR1 dehydrogenase activity. A lower inhibitory efficiency was exerted by GSDHN on the reduction of GS-nonanal (data not shown). The reductase activity of CBR1 on GSHNE and the feedback inhibitory action exerted on CBR1 by GSHDN reveals an intriguing connection between the catalytic action of CBR1 and AKR1B1, both in terms of a relative metabolic function and the applied research on AKR1B1 targeting.

Besides disclosing a special catalytic feature of hCBR1, we believe that our results open up a new front in the search for molecules able to exert anti-inflammatory activity through the inhibition of AKR1B1. In fact, if from one side targeting AKR1B1 may not be sufficient in attenuating the NF-kB activation mediated by GSDHN, on the other side the modulation of GSDHN level through

AKR1B1 inhibition may favour the detoxifying action of CBR1.

Acknowledgements. This work was supported by Pisa University, PRA 2015.

Reference

[1] Esterbauer, H.; Schauer, R. J.; Zollner, H. Chemistry and biochemistry of 4-hydroxynonenal, malonaldehyde and related aldehydes. Free Radic. Biol. Med. 11, 81-128; 1991.

[2] Halliwell, B.; Gutteridge, J.M.C., Free Radicals in Biology and Medicine second ed. Oxford: Clarendon Press; 1989.

[3] Poli, G.; Schaur, R.J. 4-Hydroxynonenal in the pathomechanisms of oxidative stress. IUBMB Life 50, 315-321; 2000.

[4] Guéraud, F.; Atalay, M.; Bresgen, N.; Cipak, A.; Eckl, P.M.; Huc, L.; Jouanin, I.; Siems, W.; Uchida, K. Chemistry and biochemistry of lipid peroxidation products. Free Radic. Res. 44: 1098-1124; 2010.

[5] Ellis, E.M. Reactive carbonyls and oxidative stress: potential for therapeutic intervention. Pharmacol. Ther. 115: 13-24; 2007.

[6] Pappa, A.; Estey, T.; Manzer, R.; Brown, D.; Vasiliou, V. Human aldehyde dehydrogenase 3A1 (ALDH3A1): biochemical characterization and immunohistochemical localization in the cornea. Biochem. J. 376: 615-623: 2003.

[7] Murphy, T.C.; Amarnath, V.; Gibson, K.M.; Picklo, M.J. Sr. Oxidation of 4-hydroxy-2-nonenal by succinic semialdehyde dehydrogenase (ALDH5A). J. Neurochem. 86: 298-305; 2003.

[8] Kong, D.; Kotraiah, V. Modulation of aldehyde dehydrogenase activity affects (±)-4-hydroxy-2E-nonenal (HNE) toxicity and HNE-protein adducts levels in PC12 cells. J. Mol. Neurosci. 47: 595-603; 2012.

[9] Vander Jagt, D. L.; Kolb, N. S.; Vander Jagt, T. J.; Chino, J.; Martinez, F. J.; Hunsaker, L. A.; Royer, R. E. Substrate specificity of human aldose reductase: identification of 4-hydroxynonenal as an endogenous substrate. Biochim. Biophys. Acta 1249:117–126; 1995.

[10] Srivastava, S.; Chandra, A.; Bhatnagar, A.; Srivastava, S. K.; Ansari, N. H. Lipid peroxidation product, 4-hydroxynonenal and its conjugate with GSH are excellent substrates of bovine lens aldose reductase. Biochem. Biophys. Res. Commun. 217:741–746; 1995.

[11] Shen, Y.; Zhong, L.; Johnson, S.; Cao, D. Human aldo-keto reductases 1B1 and 1B10: a comparative study on their enzyme activity toward electrophilic carbonyl compounds. Chem. Biol. Interact. 191 (1-3): 192-198; 2011.

[12] Hartley, D. P.; Ruth, J. A.; Petersen, D. R. The hepatocellular metabolism of 4-hydroxynonenal by alcohol dehydrogenase, aldehyde dehydrogenase, and glutathione S-transferase. Arch Biochem Biophys 316: 197−205; 1995.

[13] Guéraud, F.; Alary, J.; Costet, P.; Debrauwer, L.; Dolo, L.; Pineau, T.; Paris, A. In vivo involvement of cytochrome p450 4A family in the oxidative metabolism of the lipid preoxidation product trans-4-hydroxy-2-nonenal, using PPAR alpha-deficient mice. J. Lipid Res. 40: 152-159; 1999.

[14] Amunom, I.; Stephens, L.J.; Tamasi, V.; Cai, J.; Pierce, W.M. Jr.; Conklin, D.J.; Bhatnagar, A.; Srivastava, S.; Martin, M.V.; Guengerich, F.P.; Prough, R.A. Cytochromes p450 catalyze oxidation of alpha,beta unsatured aldehydes. Arch. Biochem. Biophys. 464: 187-196; 2007.

[15] Amunom, I.; Dieter, L-J-; Tamasi, V.; Cai, J.; Conklin, D-J.; Srivastava, S.; Martin, M.V.; Guengerich, F.P.; Prough, R.A. Cytochromes p450 catalyze the of α,β-unsatured aldehydes. Chem. Res- Toxicol. 24: 1223-1230; 2011.

[16] Hoffmann, F.; Maser, E. Carbonyl reductases and pluripotent hydroxysteroid dehydrogenases of the short-chian dehydrogenase/reductase superfamily. Drug Metab. Rev. 39: 87-144; 2007.

[17] Doorn, J.A.; Maser, E.; Blum, A.; Claffey, D.J.; Petersen, D.R. Human carbonyl reductase catalyzes reduction of 4-oxonon-2-enal. Biochemistry 43: 13106-13114; 2004.

[18] Oppermann, U. Carbonyl reductases: the complex relationships of mammalian carbonyl and quinone-reducing enzymes and their role in physiology. Annu. Rev. Pharmacol. Toxicol. 47: 293-322; 2007.

[19] Wirth, H.; Wermuth, B. Immunohistochemical localization of carbonyl reductase in human tissues. J. Histochem. Cytochem. 40: 1857-1863; 1992.

[20] Forrest, G.L.; Gonzalez, B. Carbonyl reductase. Chem. Biol. Interact. 129: 21-40; 2000.

[21] Wermuth, B. Purification and properties of an NADPH-dependent carbonyl reductase from human brain. Relationship to prostaglandin 9-ketoreductase and xenobiotic ketone reductase. J. Biol. Chem. 256: 1206-1213; 1981.

[22] Wermuth, B.; Platts, K.L.; Seidel, A,; Oesch, F. Carbonyl reductase provides the enzymatic basis of quinine detoxification in man. Biochem. Pharmacol. 35: 1277-1282; 1986.

[23] Pilka, E.S.; Niesen, F.H.; Lee, W.H.; El-Hawari, Y.; Dunford, J.E.; Kochan, G.; Wsol, V.; Martin, H.J.; Maser, E.; Oppermann, U. Structural basis for substrate specificity in human monomeric carbonyl reductases. Plos One. 4: e7113; 2009.

[24] Tinguely, J.N.; Wermuth, B. Identification of the reactive cysteine residue (Cys227) in human carbonyl reductase. Eur. J. Biochem. 260: 9-14; 1999.

[25] Feldman, R.; Luncsford, A.; Heinrikson, R.L.; Westley, J.; Jarabak, J. Glutathione-related inhibition of prostaglandin metabolism. Arch. Biochem. Biophys. 211: 375-381; 1981.
[26] Chung, H.S.; Harvey, R.G.; Armstrong, R.N.; Jarabak, J. Polycyclic aromatic hydrocarbon quinines and glutathione thioethers as substrates and inhibitors of the human placental NADP-linked 15-hydroxyprostaglandin dehydrogenase. J. Biol. Chem. 262: 12448-12451; 1987.
[27] Bateman, R.L.; Rauh, D.; Tavshanjian, B.; Shokat, K.M. Human carbonyl reductase 1 is an S-nitrosoglutathione reductase. J. Biol. Chem. 283: 35756-35762; 2008.
[28] Staab, C.A.; Hartmanová, T.; El-Hawary, Y.; Ebert, B.; Kisiela, M.; Wsol, V.; Martin, H.J.; Maser, E. Studies on reduction of S-nitrosoglutathione by human carbonyl reductases 1 and 3. Chem. Biol. Interact. 191: 95-103; 2011.
[29] Moschini, R.; Peroni, E.; Rotondo, R.; Renzone, G.; Melck, D.; Cappiello, M.; Srebot, M.; Napolitano, E.; Motta, A.; Scaloni, A.; Mura, U.; Del-Corso, A. $NADP^{(+)}$-dependent dehydrogenase activity of carbonyl reductase on glutathionylhydroxynonanal as a new pathway for hydroxynonenal detoxification. Free Rad. Biol. Med. 83: 66-76; 2015.
[30] Esterbauer, H.; Weger, W. Über die Wirkungen yon Aldehyden auf Gesunde und maligne Zellen. 3. Mitt. Monatshefte für Chemie 98: 1995-2000; 1967.
[31] Danielson, U.H.; Esterbauer, H.; Mannervik, B. Structure-activity relationships of 4-hydroxyalkenals in the conjugation catalysed by mammalian glutathione transferases. Biochem. J. 247: 707-713; 1987.
[32] Ellman, G.L. Tissue sulfhydryl groups. Arch. Biochem. Biophys. 82: 70-77; 1959.
[33] Salzano, A.M.; Renzone,G.; Scaloni,A.; Torreggiani,A.; Ferreri,C.; Chatgilialoglu, C. Human serum albumin modifications associated with reductive radical stress. Mol. Biosyst. 7: 889–898; 2011.
[34] Lirussi, L.; Antoniali, G.; Vascotto, C.; D'Ambrosio, C.; Poletto, M.; Romanello, M.; Marasco, D.; Leone, M.; Quadrifoglio, F.; Bhakat, K.K.; Scaloni, A.; Tell, G. Nucleolar accumulation of APE1 depends on charged lysine residues that undergo acetylation upon genotoxic stres and modulate its BER activity in cells. Mol. Biol. Cell 23:4079–4096; 2012.
[35] Berman, H.M.; Westbrook, J.; Feng, Z.; Gilliland, G.; Bhat, T. N.; Weissig, H.; Shindyalov, I. N.; Bourne, P. E. The Protein Data Bank. Nucleic Acids Res, 28, 235-242; 2000
[36] Case, D.A.; Berryman, J.T.; Betz, R.M.; Cerutti, D.S.; III, T.E.C.; Darden, T.A.; Duke, R.E.; Giese, T.J.; Gohlke, H.; Goetz, A.W.; Homeyer, N.; Izadi, S.; Janowski, P.; Kaus, J.; Kovalenko, A.; Lee, T.S.; LeGrand, S.; Li, P.; Luchko, T.; Luo, R.; Madej, B.; Merz, K. M.; Monard, G.; Needham, P.; Nguyen, H.; Nguyen, H.T.; Omelyan, I.; Onufriev, A.; Roe, D. R.; Roitberg, A.; Salomon-Ferrer, R.; Simmerling, C. L.; Smith, W.; Swails, J.; Walker, R.C.; Wang, J.; Wolf, R.M.;

Wu, X.; York, D.M.; Kollman, P.A. AMBER, version 14. In University of California: San Francisco, CA, 2015.

[37] Maestro, version 9.0;. In Schrödinger Inc: Portland, OR, 2009.

[38] Macromodel, version 9.7;. In Schrödinger Inc: Portland, OR, 2009.

[39] Verdonk, M.L.; Mortenson, P.N.; Hall, R.J.; Hartshorn, M.J.; Murray, C.W. Protein-ligand docking against non-native protein conformers. J. Chem. Inf. Model 48: 2214-2225; 2008.

[40] York, D.M.; Darden, T.A.; Pedersen, L.G. The effect of long-range electrostatic interactions in simulations of macromolecular crystals - a comparison of the Ewald and truncated list methods. J. Chem. Phys. 99: 8345-8348; 1993.

[41] Roe, D. R.; Cheatham, T. E., 3rd. PTRAJ and CPPTRAJ: Software for Processing and Analysis of Molecular Dynamics Trajectory Data. J. Chem. Theory Comput. 9, 3084-3095; 2013.

[42] Bradford, M.M. A rapid and sensitive method for the quantitation of microgram quantities of protein utilizing the principle of protein-dye binding. Anal. Biochem. 72: 248-254; 1976.

[43] Laemmli, U.K. Cleavage of structural proteins during the assembly of the head of bacteriophage T4. Nature 227: 680-685; 1970.

[44] Wray, W.; Boulikas, T.; Wray, V.P.; Hancock, R. Silver staining of proteins in polyacrylamide gels. Anal. Biochem. 118: 197-203; 1981.

[45] Ji, B.; Ito, K.; Suzuki, H.; Sugiyama, Y.; Horie, T. Multidrug resistance-associated protein2 (MRP2) plays an important role in the biliary excretion of glutathione conjugates of 4-hydroxynonenal. Free Radic. Biol. Med. 33: 370-378; 2002.

[46] Balogh, L.M.; Roberts, A.G.; Shireman, L.M.; Greene, R.J.; Atkins, W.M. The stereochemical course of 4-hydroxy-2-nonenal metabolism by glutathione S-transferase. J. Biol. Chem. 283: 16702-16710; 2008.

[47] Aldini, G.; Carini, M.; Beretta, G.; Bradamante, S.; Facino, R.M. Carnosine is a quencher of 4-hydroxy-nonenal: through what mechanism of reaction? Biochem. Biophys. Res. Commun. 298: 699-706; 2002.

[48] Beretta, G.; Artali, R.; Regazzoni, L.; Panigati, M.; Facino, R.M. Glycyl-histidyl- lysine (GHK) is a quencher of alpha,beta-4-hydroxy-trans-2-nonenal: a comparison with carnosine: insights into the mechanism of reaction by electrospray ionization mass spectrometry, ^{1}H NMR, and computational techniques. Chem. Res. Toxicol. 20: 1309-1314; 2007.

[49] Verdonk, M. L.; Mortenson, P. N.; Hall, R. J.; Hartshorn, M. J.; Murray, C. W. Protein-ligand docking against non-native protein conformers. J. Chem. Inf. Model 48: 2214-2225; 2008.

[50] Bohren, K.M.; von Wartburg, J.P.; Wermuth, B. Kinetics of carbonyl reductase from human brain. Biochem. J. 244: 165-171; 1987.

[51] Tammali, R.; Ramana, K.V.; Singhal, S.S.; Awasthi, S.; Srivastava, S.K. Aldose reductase regulates growth factor-induced cyclooxygenase-2 expression and prostaglandin E2 production in human colon cancer cells. Cancer Res. 66: 9705-9713; 2006.
[52] Ramana, K.V.; Bhatnagar, A.; Srivastava, S.; Yadav, U.C.; Awashti, Y.C.; Srivastava, S.K. Mitogenic responses of vascular smooth muscle cells to lipid peroxidation-derived aldehyde 4-hydroxy-trans-2-nonenal (HNE): role of aldose reductase-catalyzed reduction of the HNE-glutathione conjugates in regulating cell growth. J. Biol. Chem. 281: 17652-17660; 2006.

Figure legends

Figure 1 Kinetic analysis of hCBR1. The $NADP^+$-dependent dehydrogenase activity of hCBR1 was evaluated as described in the Methods Sections at different concentrations of either GSHNE (in the presence of 0.18 mM $NADP^+$, Panel A) or $NADP^+$ (in the presence of 0.10 mM GSHNE, Panel B). The kinetic parameters were determined by non linear regression analysis of the reported data.

Figure 2 Effect of pH on the reductase and dehydrogenase activity of hCBR1. The activity of hCBR1 was evaluated at 37 °C using 50 mM phosphate buffer at the indicated pH values and 3.2 mU/ml of hCBR1. Squares refer to the dehydrogenase activity measured in the presence of 0.18 mM $NADP^+$ and 0.10 mM GSHNE. Circles refer to the reductase activity measured in the presence of 0.18 mM NADPH and 0.03 mM GS-nonanal.

Figure 3 nLC-ESI-LIT-MS analysis of the reaction mixture containing GSHNE and NADPH. As an example the aliquot of the reaction mixture containing 50 μM GSHNE, 20 μM NADPH, 33 μM GSH, 5.5 μM HNE in 50 mM phosphate buffer, at pH 6.2, incubated with 94 mU/ml hCBR1 at 37 °C sampled after 5 min of reaction is reported. The total ion current (TIC) is showed in Panel A (the symbol § marks the peak relative to MRFA peptide (ΔRT: 18.3 min) used as internal standard). Extracted ion currents (EIC) relative to *m/z* values 464.25 (ΔRT: 30.9-34.1 min), 466.25 (ΔRT: 31.3-33.2 min), 462.23 (ΔRT: 38.0-40.1 min), 480.24 (ΔRT: 32.8-34.4 min) and 478.23 (ΔRT: 34.7 min) are showed in Panels B (the symbol ° marks the signals corresponding to the second isotope ions of the species at *m/z* 462.19), C, D, E and F, respectively. Normalized intensity levels (NL) are reported.

Figure 4. Time course of GSHNE transformation catalyzed by hCBR1. Plots of the peak areas of the molecular species at *m/z* values 464.25 (Panel A), 466.25 (Panel B), 462.23 (Panel C), 480.24 and 478.23 (Panel D, a and b plots, respectively), gained by integration of the relative extracted ion currents in LC-MS runs at different times of incubation with the hCBR1 enzyme are reported. The experimental points, reported with the corresponding error bars, are graphically interpolated in order to better visualize the trends for the concentrations of the different species during the incubation with hCBR1.

Figure 5. Extracted ion currents relative to GSHNE. The extracted ion currents (EIC) relative to *m/z* value 464.25, corresponding to GSHNE, for the 12 sampling times of the reaction mixture (see Methods for details) are shown. Reported intensities (normalized intensity levels, NL) refer to the higher peak of the triplet 1, 2, 3 and are the mean values over 5 chromatographic runs for each sampling time.

Figure 6. Minimized average structures of compounds Is and IIs docked into hCBR1. Panel A: compound **Is**; Panel B: compound **IIs**. In blue the starting docking poses for the two compound are also reported.

Figure 7. Inhibition of the dehydrogenase activity of hCBR1 by GSDHN. The dehydrogenase activity of hCBR1 was determined in standard conditions using 3.2 mU/ml of hCBR1 in the absence (●) and in the presence of the following GSDHN concentrations: (▲): 10 μM; (▼): 15 μM; (♦): 20 μM. Kinetic data are reported as double reciprocal plot. In the inset the slopes are reported in a secondary plot as a function of GSDHN concentration.

Table 1. Kinetic parameters for the reductase activity of hCBR1 on glutathionylated aldehydes.[a]

Substrate[b]	**K_M (μM)**	**k_{cat} (min^{-1})**	**k_{cat}/K_M ($mM^{-1}\,min^{-1}$)**
GS-propanal	20.7 ± 1.8	1140 ± 46	$53.1*10^3 \pm 2.3*10^3$
GS-hexanal	23.8 ± 2.7	1830 ± 101	$76.9*10^3 \pm 9.7*10^3$
GS-nonanal	6.5 ± 0.4	1848 ± 83	$276.9*10^3 \pm 21.3*10^3$
NADPH	4.5 ± 0.5	1428 ± 61	$311.1*10^3 \pm 37.2*10^3$

[a] Kinetic parameters have been obtained by non linear regression analysis of experimental data and are expressed as mean ± S.E. The assays were performed at 37 °C in 50 mM sodium phosphate buffer pH 6.0 using 3.2 mU/ml of hCBR1. Kinetic parameters for aldehydes were obtained using a fixed concentration of NADPH of 0.18 mM. Kinetic parameters for NADPH were obtained using GS-nonanal at a fixed concentration of 0.03 mM.

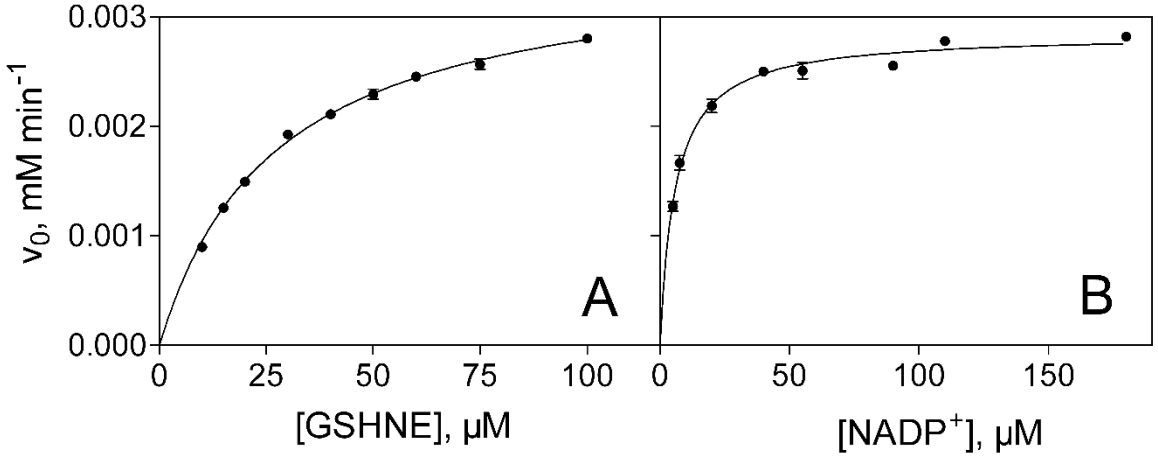

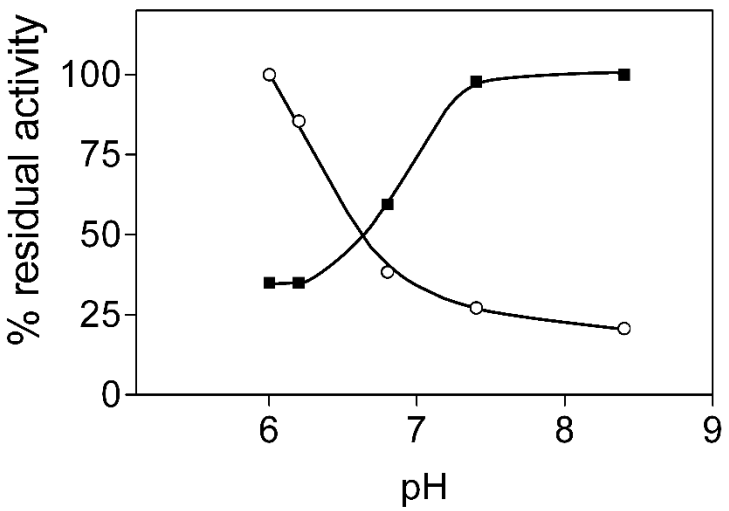
% residual activity
100
75
50
25
0
6
7
8
9
pH

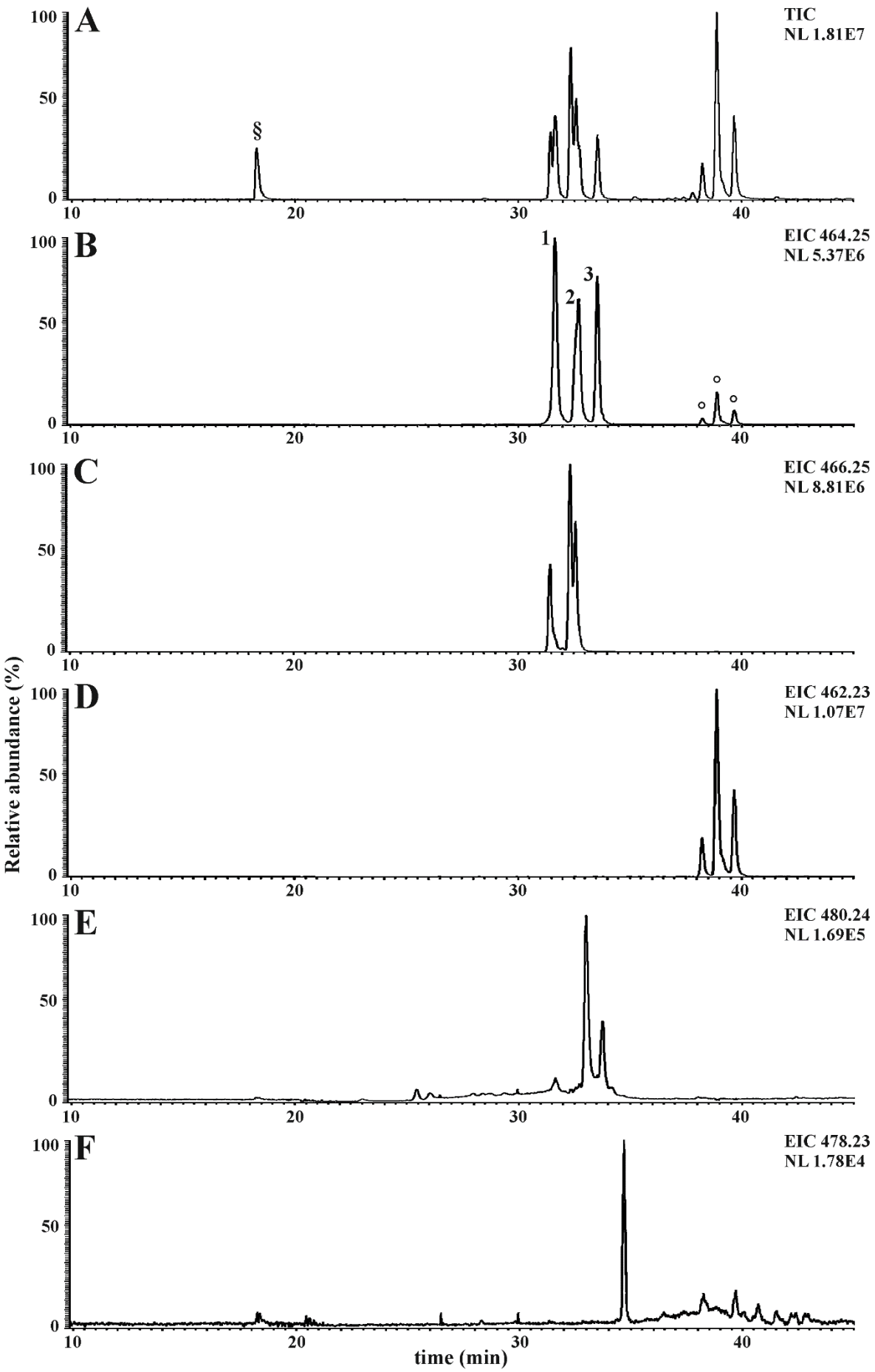
A
TIC
NL 1.81E7
§
B
EIC 464.25
NL 5.37E6
1
2
3
C
EIC 466.25
NL 8.81E6
D
EIC 462.23
NL 1.07E7
E
EIC 480.24
NL 1.69E5
F
EIC 478.23
NL 1.78E4
Relative abundance (%)
time (min)
100
50
0
10
20
30
40

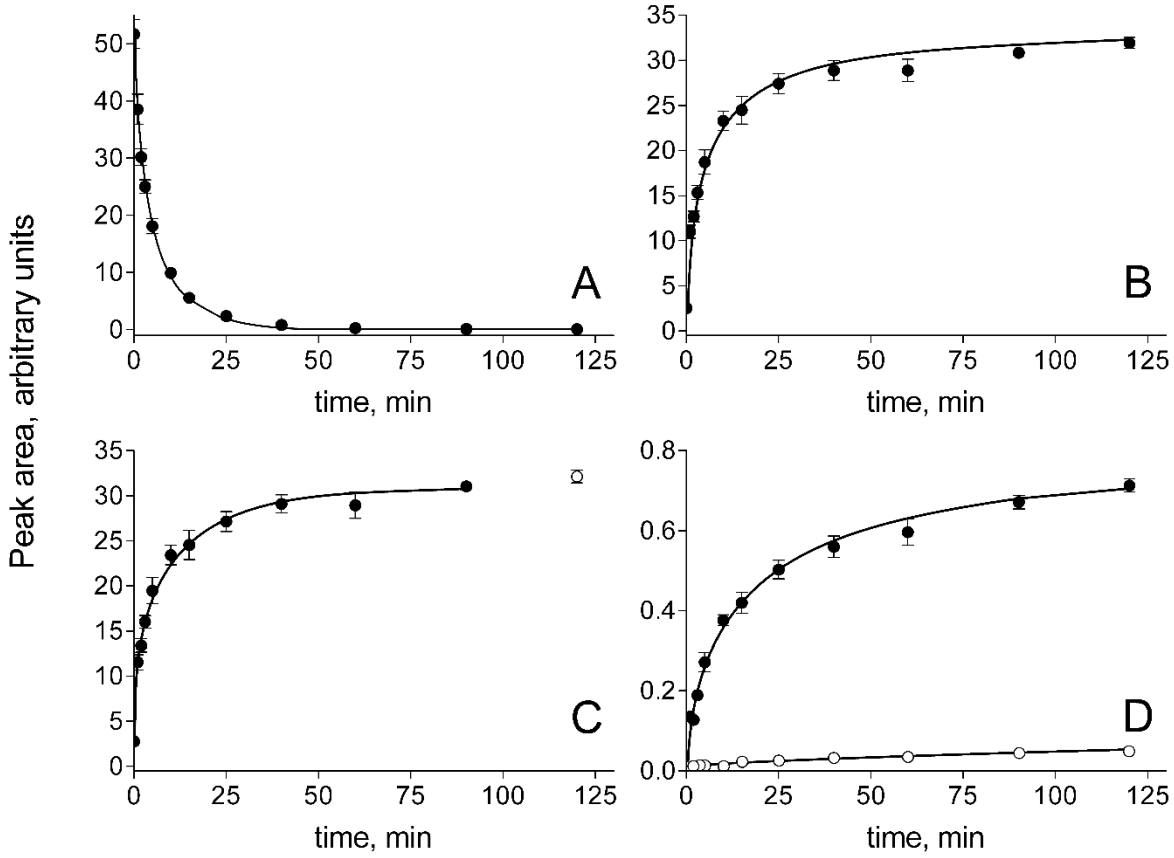
Peak area, arbitrary units
A
B
C
D
time, min
time, min
time, min
time, min

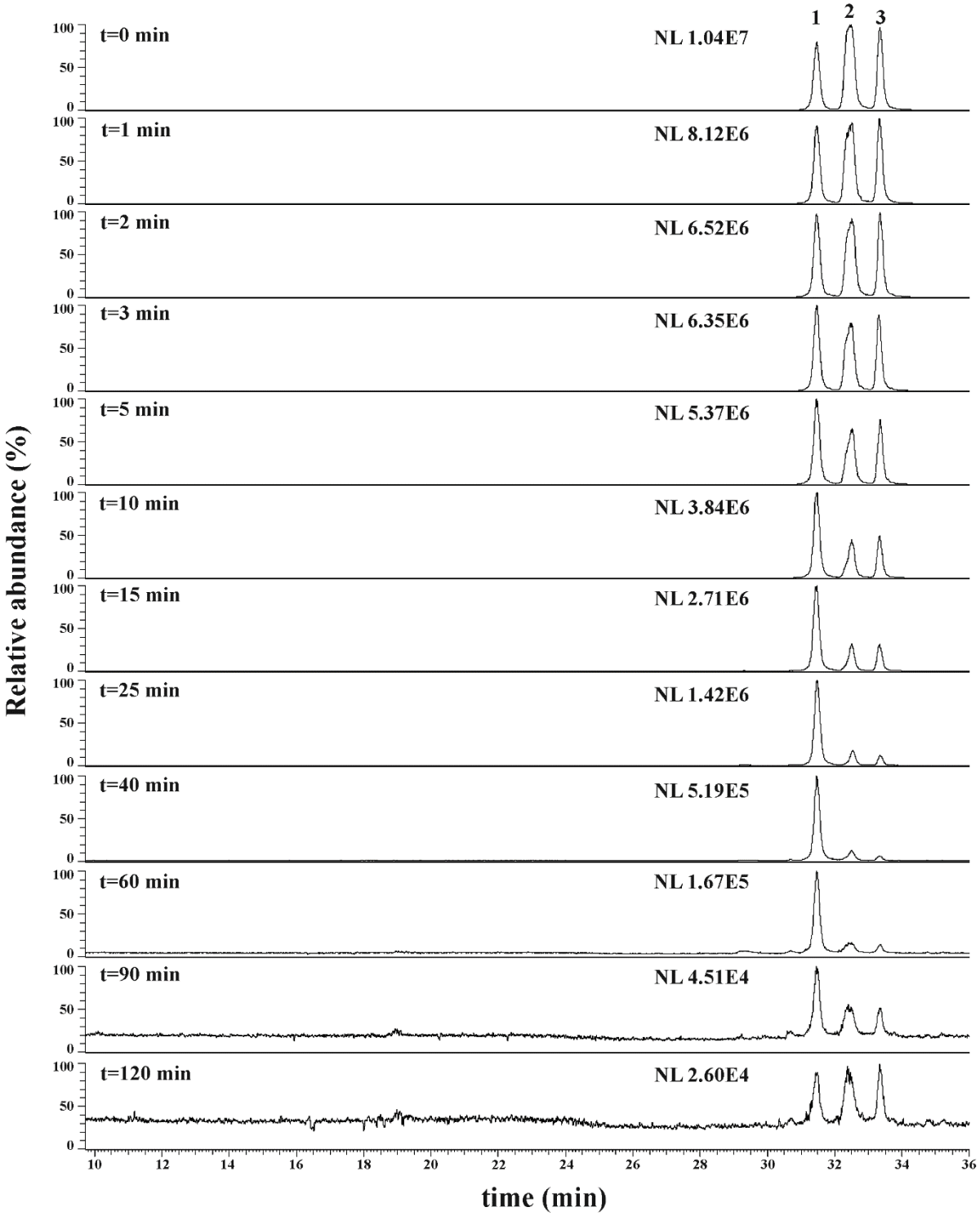
1
2
3
t=0 min
NL 1.04E7
t=1 min
NL 8.12E6
t=2 min
NL 6.52E6
t=3 min
NL 6.35E6
t=5 min
NL 5.37E6
t=10 min
NL 3.84E6
t=15 min
NL 2.71E6
t=25 min
NL 1.42E6
t=40 min
NL 5.19E5
t=60 min
NL 1.67E5
t=90 min
NL 4.51E4
t=120 min
NL 2.60E4
Relative abundance (%)
time (min)

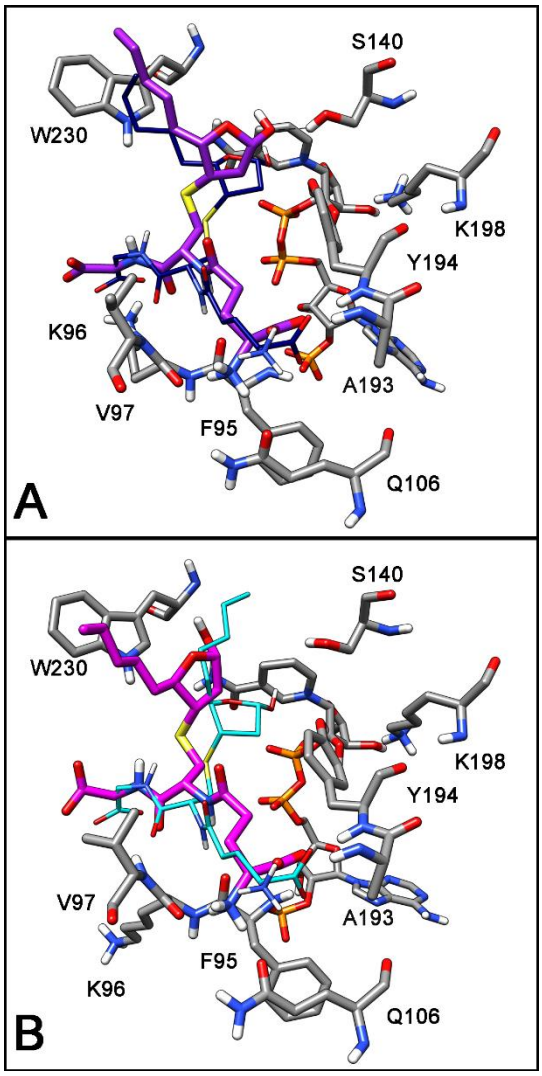
S140
W230
K198
Y194
K96
A193
V97
F95
Q106
A
S140
W230
K198
Y194
V97
A193
F95
K96
Q106
B

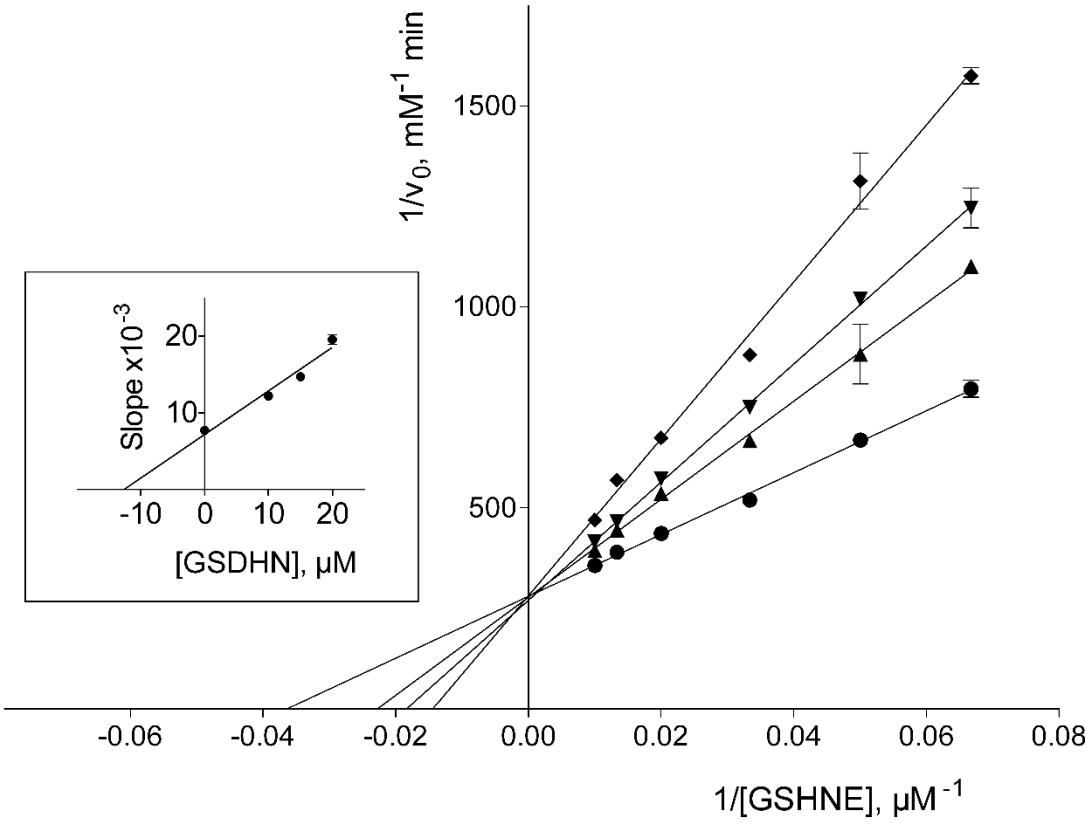
1/v0, mM-1 min
1500
1000
500
-0.06
-0.04
-0.02
0.00
0.02
0.04
0.06
0.08
1/[GSHNE], µM-1
Slope x10-3
20
10
-10
0
10
20
[GSDHN], µM